ACS OMEGA

Open Access

http://pubs.acs.org/journal/acsodf

Article

Optimizing Electrochemical Performance: A Study of Aqueous Electrolytes with Hemp-Derived Activated Carbon for Supercapacitors

Kanisorn Klangvijit, Khemjiranee Bowornthommatadsana, Mayuree Phonyiem Reilly, Teerayut Uwanno, Visittapong Yordsri, Michiko Obata, Masatsugu Fujishige, Kenji Takeuchi, and Winadda Wongwiriyapan*

Cite This: *ACS Omega* 2025, 10, 6601−6614

Read Online

ACCESS | Metrics & More | Article Recommendations | Supporting Information

ABSTRACT: This work investigates the synthesis and electrochemical performance of hemp-derived activated carbon (HAC) for supercapacitor electrode applications. HAC was prepared through NaOH chemical activation, and its electrochemical characteristics were evaluated using three different electrolytes: acidic (H_2SO_4), neutral (Na_2SO_4), and basic (KOH). The specific surface area of HAC was found to be exceptionally high, measuring 2612 m^2/g, surpassing that of commercially available activated carbon (AC). Surface analysis revealed the presence of an oxygen functional group, which provided additional pseudocapacitive active sites. When 1 M H_2SO_4 was employed as the electrolyte, HAC demonstrated a maximum specific capacitance of 594 F/g (302.4 F/cm^3) at a current density of 0.3 A/g. Notably, the HAC electrode exhibited significantly higher energy density and power density, reaching values of 82 Wh/kg (135.7 mWh/cm^3) and 188 W/kg (311 mW/cm^3), respectively, when compared to commercial AC. These results highlight the potential of HAC as a cost-effective and high-performance electrode material, particularly when paired with H_2SO_4 as the electrolyte due to their ideal micropore/mesopore ratio for H_2SO_4 electrolyte access.

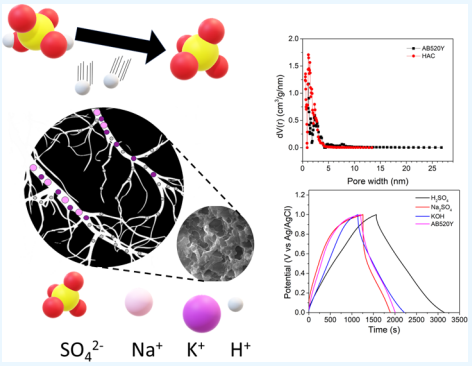

INTRODUCTION

Supercapacitors, also known as electrochemical double-layer capacitors (EDLCs), have emerged as promising energy storage solution. They operate by storing energy within an electrical double-layer formed by electrolyte ions at the interface between the electrode and electrolyte. This phenomenon has been extensively studied and documented in the literature.[1,2] Compared to lithium-ion batteries (LIBs), EDLCs demonstrate superior charge and discharge rates, cycle life,[3] and higher energy densities than traditional capacitors. Various materials, including carbon-based materials,[4−6] metal oxides,[7−12] and conductive polymers,[13−15] have been explored as electrodes for EDLCs. Among these options, activated carbon (AC) materials have garnered significant attention due to their large surface area,[16] porous structures,[17,18] favorable conductivity, and robust physical and chemical stability.[19,20]

Currently, a diverse range of carbon materials have been investigated as potential electrode materials, including AC,[21−23] template carbon,[24] carbon nanofiber,[25] carbon nanotube,[26,27] carbon aerogel,[28] and graphene.[29] AC, in particular, has been extensively utilized as an electrode material in the field of supercapacitors. Recently, a growing emphasis has been placed on synthesizing carbon-based supercapacitors using a renewable biomass-derived carbon source. Researchers have explored various biomass sources, including rice husk,[16] bamboo,[30,31] green leaves,[23,32] animal wastes,[22,33,34] and lignocellulosic materials,[35−39] for the cost-effective production of porous carbons with exceptional electrode performance.

The production of AC generally involves two main steps: first, the carbonization of raw carbon-based materials in an inert environment, followed by the activation of the carbonized material. There are two methods for activation: physical and chemical. However, chemical activation has become more widely used due to its lower temperature requirements and higher yield compared to physical activation.[40] According to previous works, alkaline hydroxides such as KOH and NaOH[5,23,41−45] are effective in producing AC with a high specific surface area. Additionally, NaOH is particularly notable because its use in activation can reduce costs and environmental impact compared to KOH.[46]

Received: August 14, 2024
Revised: November 12, 2024
Accepted: January 28, 2025
Published: February 13, 2025

Hemp (*Cannabis sativa* L.), which can grow rapidly without specific climate conditions, pesticides, or fertilizers, has been utilized for centuries. In addition to its use in textile fiber production, hemp finds applications in diverse industries such as paper manufacturing, construction materials, food production, medicine, oil extraction, and the development of biodegradable plastics. However, hemp processing generates a substantial amount of waste. Recent studies have explored the utilization of hemp fibers and stems to prepare AC for supercapacitor electrodes Hemp (*C. sativa* L.), known for its rapid growth under diverse climate conditions and minimal cultivation requirements for pesticides or fertilizers, has been utilized for centuries. Beyond its traditional use in textile fiber production, hemp has found applications in diverse industries, including paper manufacturing, construction, food production, medicine, oil extraction, and biodegradable plastics development. However, hemp processing generates substantial waste, prompting recent studies to explore the utilization of hemp fibers and stems for AC production. This AC has shown promise in supercapacitor electrodes[41,43] and adsorption applications,[42,47] benefiting from hemp's unique fibrous, hierarchical porous structure that yields high specific surface area and enhanced electrochemical properties.[48] Despite these promising applications, previous research on hemp-derived activated carbon (HAC) has predominantly utilized hydrothermal carbonization and KOH activation processes that are both time-consuming and corrosive. To address these challenges, our proposed method employs pyrolysis carbonization and NaOH activation, offering several distinct advantages. Pyrolysis carbonization is faster than hydrothermal carbonization, which involves longer reaction times at lower temperatures. The higher operating temperatures of pyrolysis carbonization result in more efficient decomposition of organic materials and fewer byproducts compared to hydrothermal methods, which involve water under high pressure. NaOH is also generally less expensive than KOH, lowering the overall production costs. Additionally, NaOH is less corrosive, reducing the risk of equipment damage and the need for specialized handling and disposal procedures. These factors make the process simpler, more cost-effective, and environmentally sustainable, offering a scalable alternative for producing HAC.

Additionally, the choice of electrolyte is critical in determining the electrochemical performance of supercapacitors.[49] Generally, liquid electrolytes fall into three main categories: aqueous, organic, and ionic. While organic electrolytes are common in commercial supercapacitors due to their larger voltage window and higher energy densities, they are not environmentally friendly. In contrast, aqueous electrolytes offer advantages such as lower cost, easier handling, and environmental friendliness, thereby simplifying supercapacitor fabrication. Aqueous electrolytes, which can be acidic, basic, or neutral, are frequently used due to their high conductivity and distinct proton transport mechanisms.[50] The ionic size of the electrolyte significantly affects capacitance;[51] smaller electrolyte ions can more easily diffuse into the electrode's pores and adsorb onto its surface, enhancing the supercapacitor's overall efficiency. Consequently, both the pore size of the electrode material and the ionic radius of the electrolyte are crucial factors in optimizing the charge storage performance.

In this work, we present the synthesis of ACs from hemp fibers (hurd and bast mixed together as received after harvest) using pyrolysis carbonization and the NaOH activation method and investigate their electrochemical properties by comparing their electrochemical performance when measured in acidic (H_2SO_4), basic (KOH), and neutral electrolyte (Na_2SO_4). The resulting HAC demonstrates a superior surface area compared to commercially available activated carbon, with oxygen functional groups present on its surface. The electrochemical analysis reveals that acidic electrolytes, such as H_2SO_4, are suitable for maximizing the electrochemical performance of the HAC for supercapacitor applications.

EXPERIMENTAL METHODS

Synthesis of Hemp-Derived Activated Carbon. The synthesis of HAC was performed by using a chemical activation method with NaOH. Initially, raw hemp fibers (husk and bast mixed together as received after harvest) were cut into small pieces and sieved using a 250 μm mesh. Subsequently, the sieved hemp fibers were dried at 80 °C for a duration of 12 h. The carbonization process was carried out to obtain biochar under a nitrogen atmosphere with a flow rate of 0.5 L/min, employing a ramping rate of 5 °C/min, and a temperature of 500 °C for 2 h. For the activation process, a mixture was prepared consisting of 1 g of biochar and NaOH at a weight ratio of biochar to NaOH 1:4. The mixture was subjected to heating at a rate of 5 °C/min under an argon atmosphere with a flow rate of 0.5 L/min, reaching a temperature of 720 °C and maintaining it for 1 h. The resulting product was a black powder. Subsequently, the black powder was treated with 1 M HCl at 100 °C for a duration of 4 h. The product was washed with deionized water until the pH reached 7, followed by drying at 100 °C for 12 h. The biochar production yield after pyrolysis was approximately 35.5%, and subsequently, the activated carbon yield after the activation process was approximately 11.4% of the original hemp fibers.

Electrode Preparation. HAC electrodes were fabricated by blending the aforementioned product with a binder (polytetrafluoroethylene: PTFE) and a carbon black in a mortar, with a ratio of 90:5:5, respectively. The mixture was thoroughly mixed for 3 min, followed by roll pressing until a desired thickness of 0.1 mm was achieved. The resulting carbon sheet was then cut into pellets with a diameter of 10 mm. These HAC pellets were subsequently heated at 80 °C overnight and stored in a desiccator with a relative humidity of less than 30%. Similarly, the commercial activated carbon electrode (AB520Y, MTI Corporation), was prepared using the same method but with substitution of the HAC with AB520Y activated carbon. The active mass of the electrode for AB520Y and HAC ranges from 5 to 7 mg/cm^2.

Material Characterization. The morphological structure of the electrodes was analyzed using a Hitachi SU5000 field emission-scanning electron microscope (FESEM) with an acceleration voltage of 5 kV. Porosity of the samples was determined by N_2 adsorption/desorption measurements at −196 °C using a Quantachrome AsiQwin instrument (Quantachrome Instruments, Florida). Prior to the measurements, the samples were degassed at 300 °C for 3.6 h. The specific surface area was calculated by using the Brunauer−Emmett−Teller (BET) equation based on the N_2 adsorption isotherm. The total pore volume was determined at a relative pressure (P/P_0) of 0.95, and the pore size distribution was analyzed using a Density Functional Theory (DFT) model. Raman spectroscopy was performed with a 532 nm laser, covering a spectral range of 50−3000 cm^{-1} (DXR SmartRa-

https://doi.org/10.1021/acsomega.4c07518
ACS Omega 2025, 10, 6601−6614

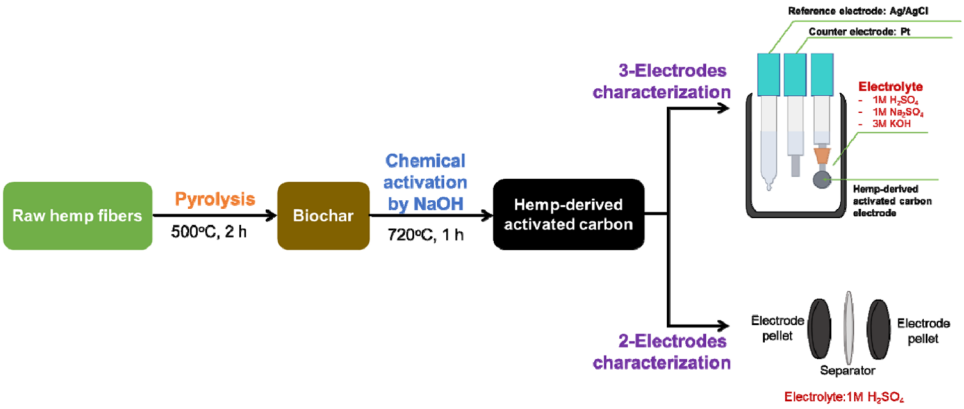

Figure 1. Overview of the entire experimental process.

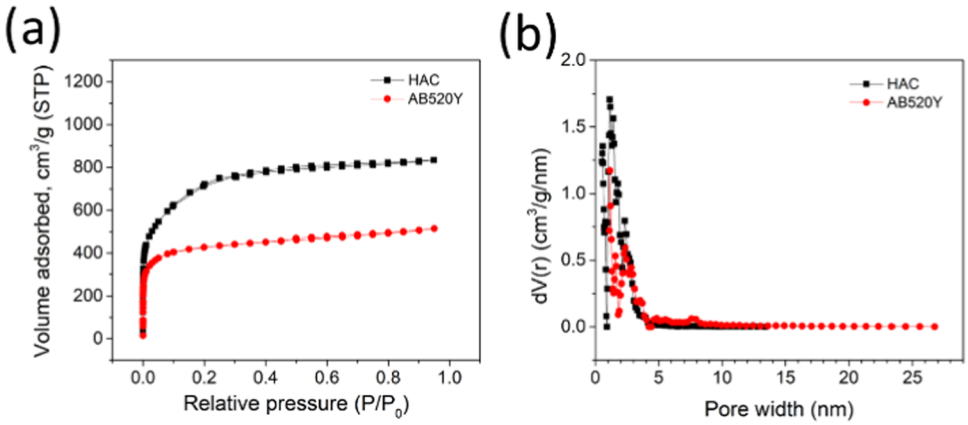

Figure 2. (a) Sorption isotherm and (b) pore size distribution of HAC and AB520Y.

man, Thermo Fisher Scientific). To investigate the carbon structure, morphology, and internal structure, a transmission electron microscope (TEM, JEOL JME-2010) was used. X-ray photoelectron spectroscopy (XPS) data were obtained by using a PHI Quantera II instrument. The radiation utilized was the Al Kα line, and the X-ray source operated at a power of 25.1 W. The C 1s peak position was calibrated to 284.6 eV and served as an internal standard for the analysis.

The electrochemical properties of the electrodes were evaluated in a three-electrode system with Ag/AgCl and a platinum sheet as reference and counter electrodes using a Metrohm Autolab PGSTAT302N instrument. Cyclic voltammetry (CV) measurements were performed by sweeping the potential in the range of −0.1 to 0.9 V vs Ag/AgCl at various scan rates for the 1 M H_2SO_4 and 1 M Na_2SO_4 electrolytes, while for 3 M KOH, the potential range was −0.9 to 0.1 V vs Ag/AgCl to prevent the oxygen evolution reaction occurring at higher potential. Galvanostatic charge−discharge (GCD) measurements were conducted by applying current in the range of 0−1.0 V vs Ag/AgCl at different current densities. Electrochemical impedance spectroscopy (EIS) was carried out over a frequency range spanning from 0.1 Hz to 100 kHz, with a voltage amplitude of 5 mV.

The specific capacitance (F/g) was determined using the following procedure

$$C = \frac{Q}{\Delta V} = \frac{1}{mv(V_1 - V_2)} \int_{V_1}^{V_2} I(V)\mathrm{d}V \quad (1)$$

The charge (Q) was calculated by integrating the area under the CV curve. Subsequently, this value was divided by the mass of the electroactive material (m, g), scan rate (v, V/s), and potential window ($\Delta V = V_1 - V_2$, V), according to eq 1.

$$C = \frac{I\Delta t}{m\Delta V} \quad (2)$$

Furthermore, eq 2 presents an alternative approach for determining the specific capacitance based on the GCD curve, where I (A) and Δt (s) denote the current and the discharging time, respectively.

The energy density (E, Wh/kg) and power density (P, W/kg) were calculated using the following eqs 3 and 4

$$E = \frac{1}{2}CV^2.\frac{1}{3.6} \quad (3)$$

$$P = \frac{E}{t} \quad (4)$$

where t is the discharge time (h).

Additionally, to demonstrate a symmetric HAC supercapacitor, a two-electrode system measurement was conducted with two symmetrical electrode pellets separated by a 30-μm-thick PTFE separator in a 1 M H_2SO_4 electrolyte. The entire experimental process is depicted in Figure 1.

RESULTS AND DISCUSSION

Figure 2a shows the nitrogen adsorption and desorption isotherm of HAC and AB520Y electrodes. The adsorption and

https://doi.org/10.1021/acsomega.4c07518
ACS Omega 2025, 10, 6601−6614

desorption isotherm is characterized as Type IV, indicating the presence of both microporous and mesoporous characteristics according to IUPAC classification.[52] This classification confirms the diverse range of pore sizes in the electrodes, which can significantly affect the ion storage and transfer properties. Figure 2b shows the pore size distribution of the electrodes. The pore diameter of HAC and AB520Y were 0.99 and 1.96 nm, respectively. This indicates that majority of the pores in the sample are micropores with a small portion of mesopore, which benefit large ion storage and high-rate ion transfer due to highly accessible surface areas.[53] Importantly, the HAC electrode exhibits micropores with a diameter approximately two times smaller than that of AB520Y, resulting in a higher specific surface area. The surface area of HAC is approximately 2612 m^2/g, while AB520Y possesses a surface area of approximately 1620 m^2/g.

Table 1 presents additional data indicating that HAC has a higher total volume, micropore surface area, and micropore volume compared to AB520Y. In general, supercapacitors store charges based on two processes: (i) electrical double-layer capacitance (EDLC) which stores physical charges (physisorption) via the formation of an electric double layer at the interface between the electrode and electrolyte, and (ii) pseudocapacitance, where the storage of electrical energy is an electrochemical process and is achieved through redox reactions, intercalation on the electrode surface by ions that are specifically adsorbed. As a high specific surface area material, AC mainly stores charges based on the EDLC process. From the previous studies, the charge storage capability of EDLC materials is largely determined by the specific surface area of the material and the effective size of the electrolyte ions, which should be in about the same size as the average pore size of the material to maximize the charge storage capability.[51] Based on the data in Table 1, the variations in pore sizes and surface areas are anticipated to have a significant impact on specific ion storage capacitance and ion transfer kinetics.

Table 1. Surface Area and Porosity Characterization of HAC and AB520Y

samples	S_{BET} (m^2/g)	S_{micro} (m^2/g)	pore diameter (nm)	V_{total} (cm^3/g)	V_{micro} (cm^3/g)
AB520Y	1621.21	1318.72	1.96	0.79	0.53
HAC	2612.88	1808.42	0.99	1.29	0.76

The morphological structure of HAC and AB520Y electrodes was characterized by FESEM as shown in Figure 3a,b. The image reveals that the HAC electrodes exhibit a sponge-like appearance with a porous structure that covers the entire surface. This porous structure plays a crucial role in facilitating easy access channels for electrolyte ions during the charge and discharge processes. In comparison, AB520Y shows a more solid, smoother surface, which offers less surface area with which electrolyte ions interact, potentially leading to lower charge storage capability. In Figure 3c,d, the microstructure of HAC and AB520Y is investigated using TEM. Both HAC and AB520Y exhibit a porous structure as fine and bright spots in the TEM images. In comparison, HAC has smaller and denser pores, which is in accordance with porosity analysis. The inset images of the selected area electron diffraction pattern (SAED) show that both HAC and AB520Y are amorphous in nature, as there are no well-defined bright spots. The crystal structure characteristics of AB520Y and HAC are further confirmed with the X-ray diffraction (XRD) technique in Figure 3e. The broad (002) diffraction peak at 2θ about 15−30° is attributed to amorphous carbon structures, while the weak and broad (101) diffraction peak of graphite structure is observed at 2θ about 40−50°.[54] Figure 3f displays the Raman spectra obtained from the HAC and AB520Y electrodes. Both spectra exhibit prominent peaks at approximately 1333 and 1594 cm^{-1}. The peak at 1333 cm^{-1} corresponds to the D band, associated with sp^3-bonded carbon atoms present in defects and disorder structures. The peak at 1594 cm^{-1} corresponds to the G band, indicating sp^2-bonded carbon atoms in hexagonal graphitic rings.[55] The intensity ratio of the D band to the G band, represented as I_D/I_G, provides valuable information about the structural properties of the samples. In the case of HAC, I_D/I_G is measured to be 0.84, whereas for AB520Y, I_D/I_G is found to be 1.13. The lower I_D/I_G value observed in HAC indicates a more ordered structure that ensures its low electrical resistance during the charge−discharge process.

The surface chemistry of HAC and AB520Y was characterized by XPS. Figure 4a displays the XPS survey spectra obtained from HAC and AB520Y. Due to the low percentage of nitrogen functional groups on the surface of HAC and AB520Y, the nitrogen peak is nearly indistinguishable in the XPS survey spectrum. The atomic percentages of the elements present on the surface of the samples are summarized in Table 2. Comparing the two samples, HAC exhibits a higher atomic percentage of oxygen and nitrogen, measuring 7.97 and 1.23%, respectively, while AB520Y shows slightly lower values of 6.67% for oxygen and 0.73% for nitrogen. This variation in the elemental composition may have implications for the surface properties and performance of the supercapacitor electrodes. Figure 4b,c illustrates the XPS C 1s spectra of HAC and AB520Y. The deconvolution of the C 1s peak reveals four distinct peaks with binding energies at 284.5, 286.4, 287.8, and 289.1 eV, corresponding to different carbon species;[56,57] C−C/C═C in aromatic rings, C−OH for epoxy and alkoxy groups, C═O for carbonyl groups, and O═C−OH carboxylate carbon, respectively. The relative percentages of these oxygen functional groups are higher in HAC compared to those in AB520Y, as summarized in Table 3. The higher presence of oxygen functional groups, albeit in relatively low concentrations, in HAC suggests the incorporation of hydrophilic species on the materials surface. These oxygen-rich functional groups contribute to the hydrophilic properties of the electrodes, promoting better electrolyte wetting and enhancing ion accessibility during charge and discharge processes. Additionally, these functional groups are expected to provide additional specific capacitance to the supercapacitor, potentially enhancing its overall performance.

Electrochemical Characterization. The electrochemical properties of HAC were measured in a three-electrode system using 1 M H_2SO_4, 1 M Na_2SO_4, and 3 M KOH as acidic, neutral, and basic electrolytes, respectively. Additionally, the commercialized AC, AB520Y, was employed as a reference for the HAC electrode in the H_2SO_4 electrolyte. The specific capacitance was calculated from both cyclic voltammetry (CV) and galvanostatic charge−discharge (GCD) curves. CV is a technique utilized to investigate the electrochemical behavior of electrode materials by measuring current as a function of applied potential. Figure 5a displays the CV curves of HAC obtained at a scan rate of 5 mV/s using different electrolytes,

https://doi.org/10.1021/acsomega.4c07518
ACS Omega 2025, 10, 6601−6614

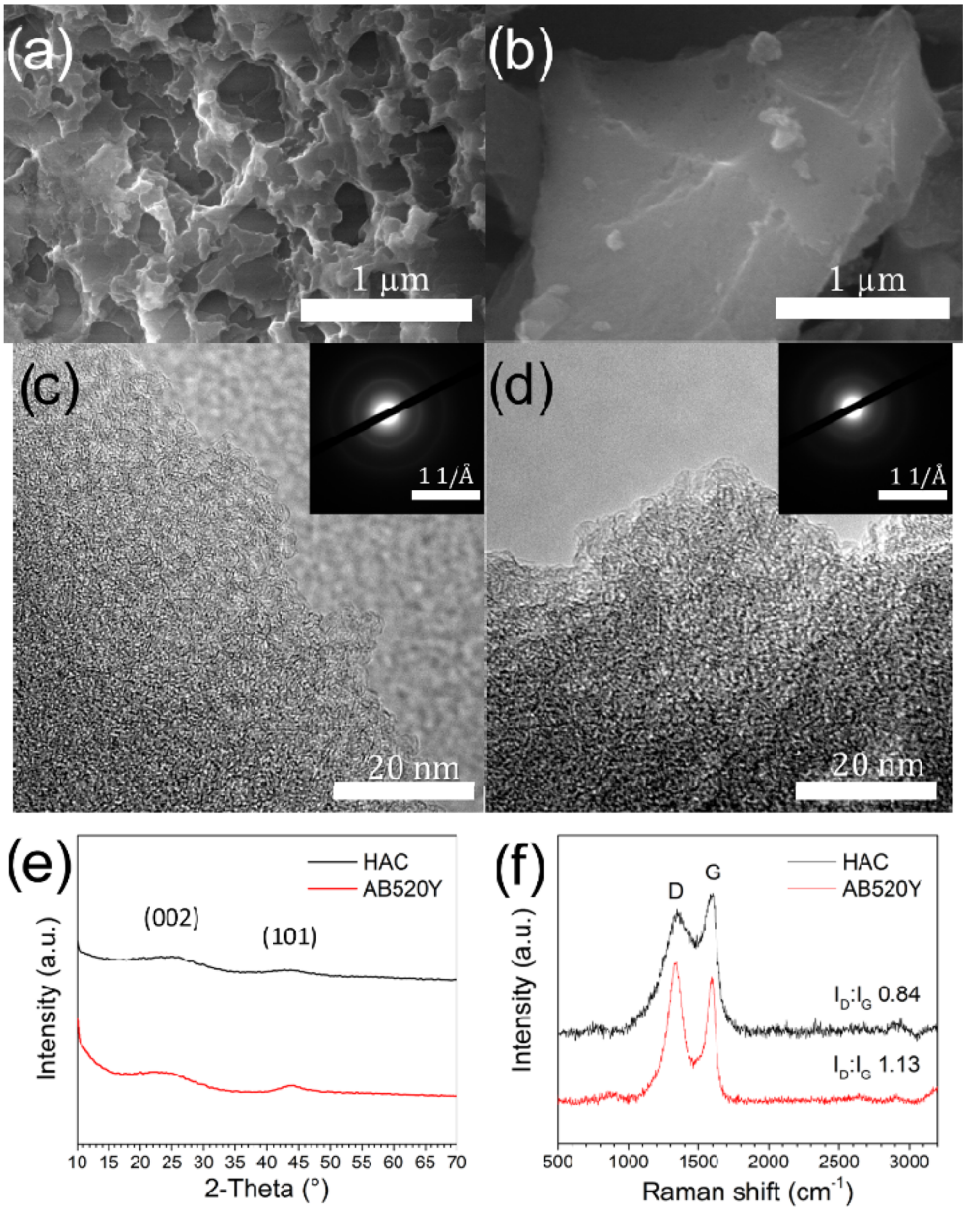

Figure 3. FESEM and TEM images of (a, c) HAC and (b, d) AB520Y. (e) XRD patterns and (f) Raman spectra of the HAC and AB520Y electrodes.

along with the comparison of AB520Y in the H_2SO_4 electrolyte.

The CV curves exhibit a relatively rectangular shape, indicative of a dynamically reversible process, except for the 1 M Na_2SO_4 electrolyte. Furthermore, the electrode demonstrates pseudocapacitive behavior, characterized by a pair of redox-reduced peaks originating from rapid and reversible reactions occurring on the surface of the active material.[58,59] The selected potential range of −0.9 to 0.1 V for 3 M KOH is optimized for the stability of the electrolyte and electrode during the charge and discharge processes.[60] Notably, HAC measured in 1 M H_2SO_4 electrolyte exhibits the highest specific capacitance, as evidenced by its largest enclosed curve area, followed by that in 3 M KOH and 1 M Na_2SO_4, respectively. The CV curve of the HAC electrode measured in 1 M Na_2SO_4 exhibited an elliptical shape, even at a low scan rate of 5 mV/s. This may be attributed to the relatively large size of the electrolyte ions (Na^+ and SO_4^{2-}) compared with other electrolytes, resulting in limited ion accessibility to the pores and consequently higher charge transfer resistance, as evidenced in the EIS spectra. The calculated specific capacitances of HAC in 1 M H_2SO_4, 3 M KOH, and 1 M Na_2SO_4 electrolytes at a scan rate of 5 mV/s are 571 F/g (290.7 F/cm^3), 413 F/g (252.3 F/cm^3), and 240 F/g (189.4 F/cm^3), respectively. In comparison, AB520Y shows a significantly smaller enclosed curve area, suggesting a lower specific capacitance resulting from a lower surface area according to porosity analysis (292 F/g (219.3 F/cm^3) at 5 mV/s). Moreover, when measured in 1 M H_2SO_4 electrolyte, HAC demonstrates pseudocapacitive characteristics within the potential range of 0−0.6 V, which are suggested to be attributed to the incorporation of oxygen functional groups on the electrode surface.[61]

The GCD curves of HAC measured with 3 different electrolytes at a current density of 0.3 A/g, along with the AB520Y electrode, are shown in Figure 5b. The GCD curves of

https://doi.org/10.1021/acsomega.4c07518
ACS Omega 2025, 10, 6601−6614

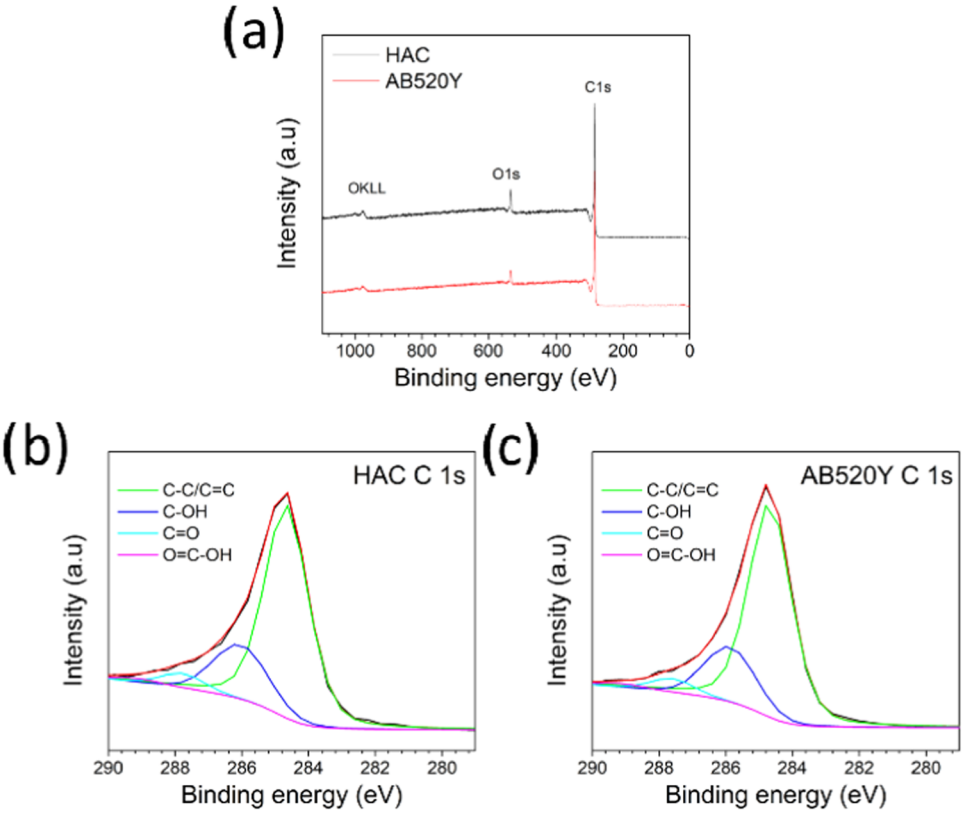

Figure 4. (a) XPS survey spectra of the HAC and AB520Y electrode material. High-resolution C 1s XPS spectra of (b) HAC and (c) AB520Y.

Table 2. Atomic Percentages of the Elements Found on the Surfaces of the HAC and AB520Y Electrode Material

	elements (atom %)		
samples	C	O	N
HAC	90.8	7.97	1.23
AB520Y	92.6	6.67	0.73

Table 3. Percentage Contents of Carbon Species Present in the Electrode Materials Based on C 1s Spectra

	carbon species (atom %)			
samples	C−C/C=C	C−OH	C=O	O=C−OH
HAC	73.25	21.01	4.48	1.27
AB520Y	73.93	20.82	4.13	1.12

HAC displayed an almost symmetrical triangle with a small voltage drop when measured in 1 M H_2SO_4 and 3 M KOH, indicating highly reversible properties. These curves show a nearly linear correlation between the potential and time, clearly demonstrating the electrochemical double-layer characteristics of the electrode. In contrast, HAC measured in 1 M Na_2SO_4 exhibited a much larger voltage drop, indicating the high electrical resistance of the electrode, which resulted in lower charge storage efficiency. The charge storage efficiency of HAC in 1 M H_2SO_4, 3 M KOH, and 1 M Na_2SO_4 were approximately 65, 59 and 22%, respectively. The slight variation of slope was caused by the pseudocapacitive nature of oxygen functional groups on the surface of the electrode. This is attributed to the charge storage through the process of adsorption/desorption at the interface of the electrode and electrolyte.[62] The sharp drop at the beginning of the discharging segment was a voltage drop due to the intrinsic electrical resistance of the materials. The specific capacitances of HAC in 1 M H_2SO_4, 3 M KOH, and 1 M Na_2SO_4 electrolytes at a current density of 0.3 A/g are 594 F/g (302.4 F/cm^3), 436 F/g (266.3 F/cm^3), and 304 F/g (239.9 F/cm^3), respectively. Notably, the specific capacitance of HAC in 1 M H_2SO_4 is the highest, with a value almost 2 times higher than that of AB520Y measured in the same electrolyte (295 F/g (221.5 F/cm^3) at 0.3 A/g). The highest specific capacitance may be attributed to the presence of oxygen-functionalized groups, a high surface area, and an optimum pore size.

The oxygen functional groups present in the aqueous electrolytes are primarily involved in these reactions as shown in eqs 5−7[63−66]

$$C - OH \leftrightarrow C = O + H^+ + e^- \quad (5)$$

$$-COOH \leftrightarrow COO + H^+ + e^- \quad (6)$$

$$C = O + e^- \leftrightarrow C - O \quad (7)$$

Equations 5 and 6 exhibit quasi-reversible or irreversible characteristics mainly in alkaline and neutral electrolytes, while the faradaic pseudocapacitance primarily originates from eq 7. It is noteworthy that the presence of oxygen functional groups can enhance the interfacial wetting properties between the electrode material and the electrolyte. Furthermore, the presence of oxygen functional groups with an excess free electron not only enhances the wetting properties but also induces faradaic pseudocapacitance within the aqueous electrolyte.[63,66] This characteristic renders HAC a promising candidate as an electrode material in supercapacitors.[67]

EIS technique was utilized to complete the electrochemical characterization of HAC and AB520Y electrodes and to gain a

https://doi.org/10.1021/acsomega.4c07518
ACS Omega 2025, 10, 6601−6614

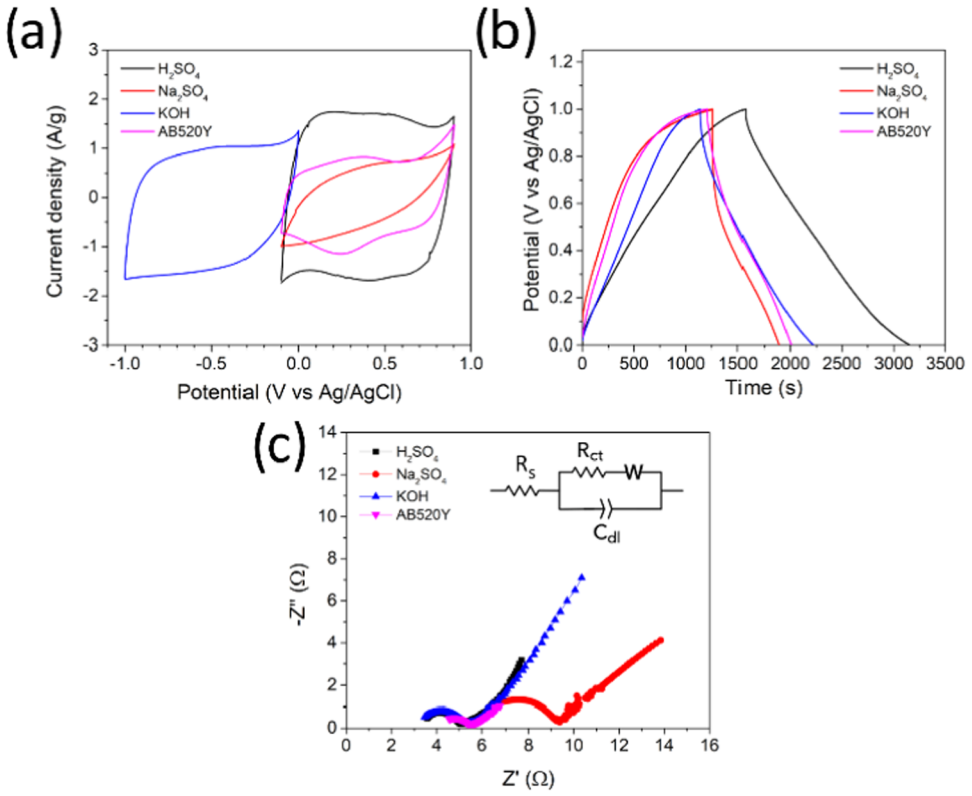

Figure 5. (a) Cyclic voltammetry curves of HAC electrode in different electrolytes and AB520Y electrode in 1 M H_2SO_4 electrolyte at scan rate 5 mV/s. (b) Galvanic charge−discharge curves of HAC electrode in different electrolytes and AB520Y electrode in 1 M H_2SO_4 electrolyte at current density 0.3 A/g. (c) Electrochemical impedance spectroscopy curve of HAC in different electrolytes and AB520Y electrode in 1 M H_2SO_4 electrolyte.

better understanding of their performance and energy storage mechanism. EIS is a highly effective method for analyzing electrochemical processes that take place at various frequencies in supercapacitors. The use of an EIS technique enables a comprehensive analysis of the frequency response characteristics of the systems, thereby furnishing valuable insights into their resistive and capacitive attributes. The resistive processes that take place in supercapacitors, namely, series resistance (R_S) and charge transfer resistance at the electrode/electrolyte interface (R_{CT}), can be discerned by studying three distinct frequency zones in the Nyquist plot. The starting point of intersection of the *x*-axis is primarily ascribed to R_S resulting from various contacts, particularly the measurement contact, the contact resistance between the electrode material and the current collector, and the resistance of the bulk electrolyte.[68] R_{CT} due to charge transfer at the interface between the electrode surface and the electrolyte can be determined as the diameter of the semicircle at higher frequencies. At lower frequencies, ion diffusion becomes the primary contributor. This results in ions being able to penetrate deeper into the pores of the carbonaceous material, leading to an increased path length for the ions in the electrolyte. EIS curves of HAC in different electrolytes and AB520Y are shown in Figure 5c, with the equivalent circuit model shown in the inset of Figure 5c, where C_{dl} and W are the electrical double-layer capacitance and Warburg impedance, respectively. The fitted values of R_S, R_{CT}, C_{dl}, and W obtained from the equivalent circuit model based on EIS spectra are compared in Table 4.

For HAC measured in 1 M H_2SO_4 and 3 M KOH electrolytes, values of R_S and R_{CT} were approximately 2.9 and 1.7 Ω for H_2SO_4, and 3.1 and 2.1 Ω for KOH, respectively. In contrast, the AB520Y electrode measured in 1 M H_2SO_4 has a higher R_S of 4 Ω but a lower R_{CT} of 1.5 Ω. For the HAC electrode measured in 1 M Na_2SO_4 electrolyte, both R_S (5.6 Ω) and R_{CT} (3.7 Ω) values were significantly higher compared to those measured in H_2SO_4 and KOH. The relatively low R_S and R_{CT} values of H_2SO_4 and KOH suggest good ionic conductivity and charge transfer capabilities for these electrolytes. A relatively high W observed with H_2SO_4 compared to KOH for both HAC and AB520Y may be attributed to several factors such as ion size, electrolyte conductivity, and ion mobility. Although H^+ ions are smaller and generally have higher ionic conductivity compared to K^+ ions, the SO_4^{2-} ions are larger and have lower ionic conductivity compared to that of OH^- ions. Furthermore, the concentration of KOH (3 M) is higher than that of H_2SO_4 (1 M). These factors may enable KOH to better penetrate narrow pore entrances and form an electrical double-layer capacitance, resulting in a lower W.

The superiority of HAC electrochemical performance in the H_2SO_4 electrolyte was likely due to the size of the hydrated ions of the electrolyte. The pure ionic radius, when not

Table 4. Comparison of Fitted Values for R_S, R_{CT}, C_{dl}, and W Obtained from the Equivalent Circuit Model Based on EIS Spectra

samples	R_s (Ω)	R_{CT} (Ω)	C_{dl} (μF)	W ($m\Omega^{-1}$ $s^{1/2}$)
HAC − H_2SO_4	2.9	1.7	9.97	448
HAC − KOH	3.1	2.1	7.25	115
HAC − Na_2SO_4	5.6	3.7	1.45	121
AB520Y − H_2SO_4	4.0	1.5	4.48	294

https://doi.org/10.1021/acsomega.4c07518
ACS Omega 2025, 10, 6601−6614

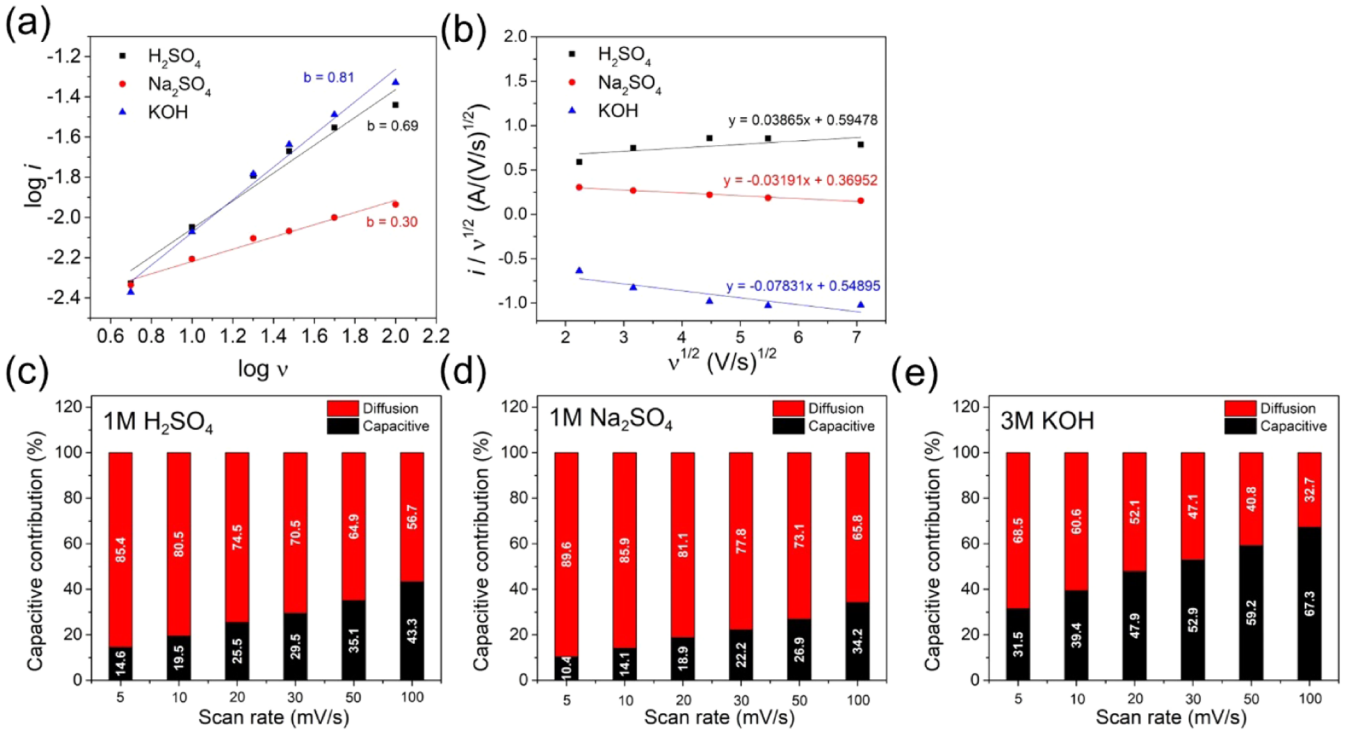

Figure 6. Evaluating the contribution from capacitive and diffusion-controlled current toward total current. (a) Plot of log i vs log ν for determining the slope b. (b) Plot of $i/\nu^{(1/2)}$ vs $\nu^{(1/2)}$ for determining k_1 and k_2 values. Capacitive and diffusion-controlled contributions at different scan rates in (c) 1 M H_2SO_4, (d) 1 M Na_2SO_4, and (e) 3 M KOH electrolytes.

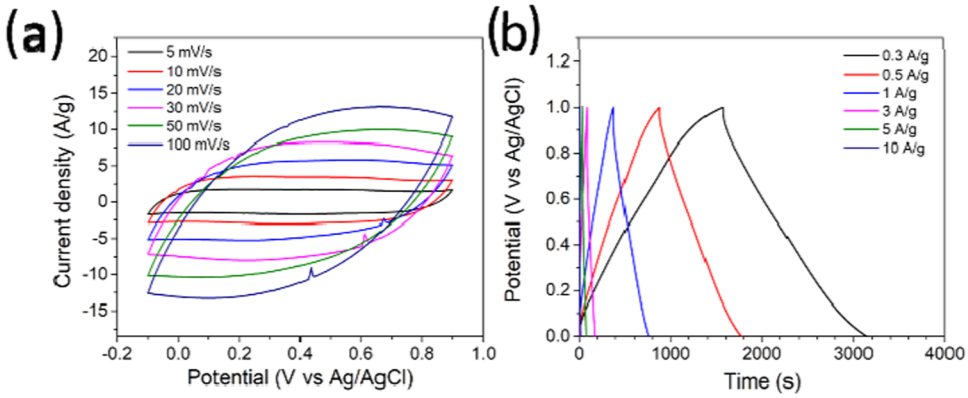

Figure 7. (a) Cyclic voltammetry curves of HAC electrode in 1 M H2SO4 electrolyte at different scan rates. (b) Galvanostatic charge−discharge curves of HAC electrode in 1 M H_2SO_4 electrolyte at different current densities.

considering other factors, is the focal point of the Coulomb force utilizing the formula $F = KQ_1Q_2/r^2$, where F represents the Coulomb force, r is the distance between two charges (Q_1 and Q_2), and K is the Coulomb constant. The hydrated ionic radius increases as more water molecules combine with the stronger Coulomb force. The hydrated ionic radius of H^+, Na^+, and K^+ was 2.80, 3.58, and 3.31 Å, respectively.[69,70] The Na_2SO_4 electrolyte, which contains both Na^+ and SO_4^{2-}, and has a larger ionic size, posed a disadvantage for charge storage at the electrode/electrolyte interface.[71,72] The KOH electrolyte, with a hydrated ionic radius of 3.31 Å, was found to be the most suitable for AC with a mesoporous structure.[73,74] When compared to the average pore size of HAC, which consists mainly of micropores (0.99 nm), the H_2SO_4 electrolyte is the most suitable due to the approximately same size of the hydrated ions and the pore size.[4,75]

Furthermore, the kinetics of the charge storage mechanism can be studied by analyzing the CV curves of the sample measured at different scan rates (5−100 mV/s). According to the Dunn model, the total stored charge can be separated into two components: the capacitive (surface-induced) and diffusion-controlled (insertion/extraction) process.[76] The power law is used to explain the relationship between the measured current (i) and the scan rate (ν)

$$i = a\nu^b \tag{8}$$

Here, a and b are adjustable parameters, with b-value determined from the slope of the log i vs log ν plot. Two specific conditions are defined: for b = 0.5, the current is proportional to the square root of the scan rate, aligning with the Cottrell equation and suggesting a predominant diffusion contribution (battery-like behavior). For b = 1, the charge

https://doi.org/10.1021/acsomega.4c07518
ACS Omega 2025, 10, 6601−6614

Table 5. Comparison of the Electrochemical Performance of the Hemp-Derived Activated Carbon Electrode

electrode materials	activation conditions	specific capacitance	electrolyte	window voltage (V)	references
durian husk	NaOH ratio: 1:2.5 720 °C, 1 h	136.5 F/g @ 1 A/g	1 M Na_2SO_4	1	5
poplar catkins	KOH ratio: 1:4 800 °C, 1 h	314 F/g @ 1 A/g	1 M Na_2SO_4	1	17
banana leaves	K_2CO_3 ratio: 1:2 750 °C, 5 h	55 F/g @ 1 A/g	0.5 M Na_2SO_4	1.2	18
Samanea saman leaves	NaOH ratio: 1:2 720 °C, 1 h	155 F/g @ 0.5 A/g	1 M $TEABF_4$	2.5	23
blackfish bone	KOH ratio: 1:3 600 °C, 1 h	251 F/g @ 1 A/g	6 M KOH	1	33
wheat straw	H_2SO_4 ratio: 1:3 800 °C, 2 h	162 F/g @ 2 mA/cm^2	2 M NaOH	1	37
wheat straw	KOH ratio: 1:3 800 °C, 2 h	106 F/g @ 2 mA/cm^2	2 M NaOH	1	37
hemp straw	KOH ratio: 1:4 800 °C, 1 h	279 F/g @ 0.5 A/g	6 M KOH	1	41
hemp hurd	KOH ratio: 1:5 800 °C, 1 h	167 F/g @ 1 A/g	1.8 M $TEMABF_4$/PC	2.5	43
hemp stems	NaOH 700 °C, 2 h	123 F/g @ 1A/g	6 M KOH	0.8	44
hemp fiber	CO_2 activation	475 F/g @ 1 A/g	PVA-KOH	1	78
hemp	KOH ratio: 1:2 800 °C, 2 h	145 F/g @ 1A/g	6 M KOH	1.1	79
HAC	NaOH ratio: 1:4 720 °C, 1 h	594 F/g @ 0.3 A/g 477 F/g @ 1.0 A/g	1 M H_2SO_4	1	this work
HAC		436 F/g @ 0.3 A/g 340 F/g @ 1.0 A/g	3 M KOH	1	this work
HAC		304 F/g @ 0.3 A/g 174 F/g @ 1.0 A/g	1 M Na_2SO_4	1	this work

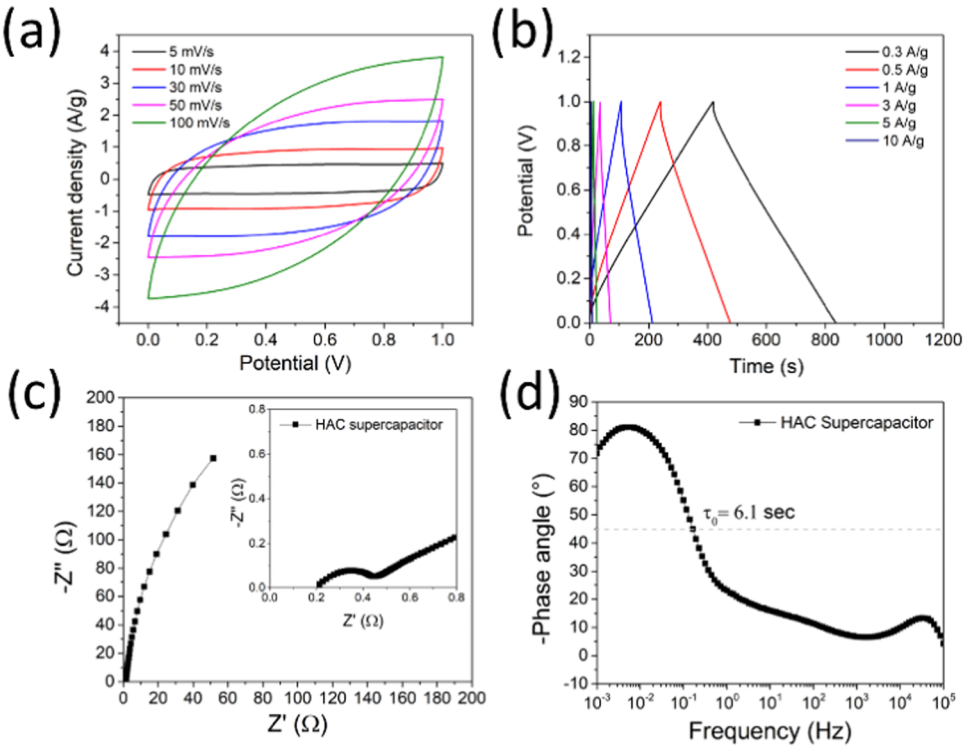

Figure 8. (a) Cyclic voltammetry and (b) galvanostatic charge−discharge curves along with (c) Nyquist and (d) and Bode plots of a symmetric HAC supercapacitor using 1 M H_2SO_4 as an electrolyte.

storage is characterized by a capacitive contribution (capacitor-like behavior).[77] Figure 6a depicts a plot of log i vs log ν to determine the slope b. The b-values obtained from 1 M H_2SO_4, 1 M Na_2SO_4, and 3 M KOH electrolytes are 0.69, 0.30, and 0.81, respectively, indicating a hybrid charge storage mechanism in the cases of 1 M H_2SO_4 and 3 M KOH.

The quantitative contribution of the capacitive- and diffusion-controlled process can be further analyzed at a fixed potential (V) and calculated using the following equation[77]

$$i(V) = k_1\nu + k_2\nu^{1/2} \quad (9)$$

where i represents the total current at a fixed potential, with $k_1\nu$ and $k_2\nu^{1/2}$ representing the current contributions from the capacitive (including both pseudocapacitance and EDLC) and the diffusion-controlled processes, respectively. The parameters k_1 and k_2 can be derived from the slope and the intercept of the y-axis of straight-line plots of $i(V)/\nu^{1/2}$ vs $\nu^{1/2}$, as illustrated in Figure 6b. By determination of the k_1 and k_2 values, it is possible to differentiate the capacitive and diffusion contributions to the total current response. Figure 6c,d displays the ratio capacitive to diffusion contributions at scan rates ranging from 5 to 100 mV/s for 1 M H_2SO_4, 1 M Na_2SO_4, and 3 M KOH electrolytes, respectively. Notably, the ratio of the capacitive contribution increases with higher scan rates.

Figure 7a,b displays CV and GCD curves of HAC measured in 1 M H_2SO_4 at different scan rates and different current densities. At low scan rates and current densities, the HAC electrode can demonstrate full electrochemical performance.

https://doi.org/10.1021/acsomega.4c07518
ACS Omega 2025, 10, 6601−6614

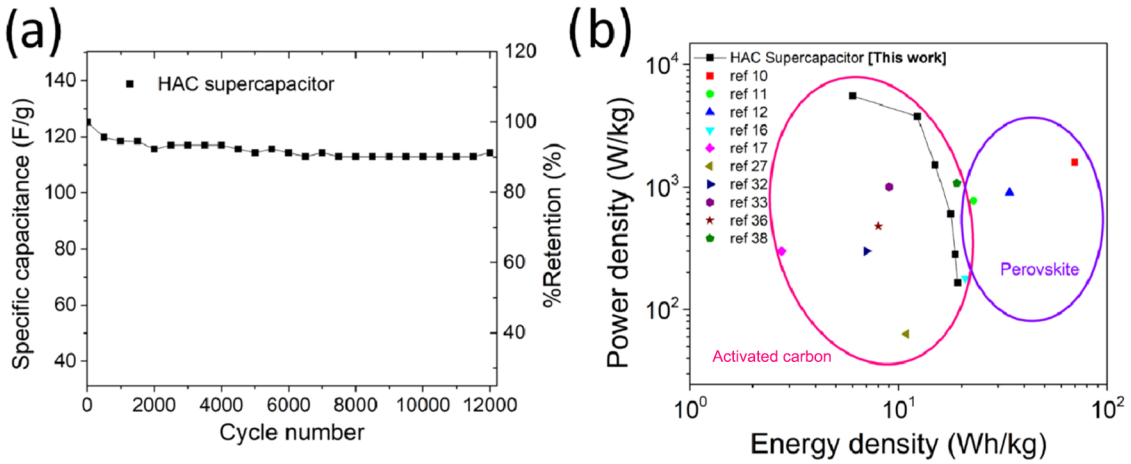

Figure 9. (a) Cycling performance test of HAC supercapacitor with 1 M H_2SO_4 electrolyte by repeating galvanostatic charge−discharge at current density 0.3 A/g for 12,000 cycles. (b) Ragone plot comparing HAC supercapacitor with activated carbon from various biomasses and high-end metal oxide research.

However, at higher scan rates and current densities, the high electrical resistance and small average pore size prevent HAC from fully using its surface area. This limitation occurs because the electrolyte ions cannot be efficiently transported into the inner surfaces of the porous structure, thereby reducing the charge storage capability. HAC electrode achieved the highest energy density of 82 Wh/kg (135.7 mWh/cm^3) with a power density of 188 W/kg (311.1 mW/cm^3), whereas the AB520Y electrode had an energy density of 41 Wh/kg (30.7 mWh/cm^3) and a power density of 184 W/kg (138.2 mW/cm^3). Furthermore, when compared to recently studied hemp-activated carbon, the specific capacitance of the work in this study was relatively high, as indicated in Table 5. This implies a promising potential for using HAC as a high-performance supercapacitor.

The electrochemical properties of HAC electrodes in a 1 M H_2SO_4 electrolyte were further explored by assembling a symmetric supercapacitor by using two HAC electrodes and a PTFE membrane as the separator. The CV and CD curves for this HAC supercapacitor are presented in Figure 8a,b. The HAC supercapacitor exhibited good stability with increasing scan rates and current densities. The efficiency of the HAC supercapacitor calculated from the CD curve is approximately 84.06%, which aligns with the efficiencies reported in previous studies. This efficiency level suggests that while some irreversible processes are present, as is typical in practical applications, the performance of our supercapacitor remains within the expected range for this configuration. The specific capacitance of the HAC supercapacitor, measured at a current density of 0.3 A/g, was approximately 138 F/g (228.3 F/cm^3). Additionally, the maximum energy density and power density achieved were 19 Wh/kg (31.4 mWh/cm^3) and 165 W/kg (273 mW/cm^3), respectively. To facilitate a more comprehensive examination of the EIS test across a frequency range from 1 mHz to 100 kHz, the Nyquist plot for the HAC supercapacitor (Figure 8c) shows low R_S and R_{CT} values of 0.21 and 0.22 Ω, respectively. Additionally, the Bode plot (Figure 8d) illustrates the relationship between the frequency and phase angle of the HAC supercapacitor. It is well-known that capacitive behavior is improved as the phase angle approaches 90°. The phase angle achieved by the HAC supercapacitor is −81.1°, indicating significant capacitive behavior. Additionally, a comparison between the characteristic frequency (f_0), which is the frequency at a phase angle of 45°, and the relaxation time constant ($\tau_0 = 1/f_0$) helps evaluate the frequency response of the supercapacitors. The relaxation time constant (τ_0) represents the minimum duration required for the device to completely discharge its energy if its efficiency exceeds 50%. The Bode plot in Figure 8d shows that the HAC supercapacitor has a f_0 value of 163.8 mHz, equivalent to a time constant of 6.1 s. Additionally, the Bode plots of the HAC electrode measured in various electrolytes are presented in Figure S1 for comparison. The HAC electrode measured in 1 M H_2SO_4 electrolyte exhibited a significantly shorter relaxation time (∼91 s) compared to the other two electrolytes. This is likely due to the smaller size of the hydrated ions in H_2SO_4, which can be more easily transported through the microporous structure of the HAC electrode. Furthermore, the HAC supercapacitor demonstrated an even shorter relaxation time than the HAC electrode (∼6.1 s), indicating considerably lower electrical resistance in the HAC supercapacitor.

A durability test was conducted over 12,000 cycles for the HAC supercapacitor using 1 M H_2SO_4 electrolyte at a current density of 0.3 A/g. After 500 cycles, the specific capacitance of the HAC supercapacitor remains at approximately 95% of its initial value and gradually decreases to 91% after 12,000 cycles, demonstrating good stability and retention of capacitance (Figure 9a). Figure S2 illustrates the specific capacitance retention of the HAC electrodes (Figure S2a) and the HAC supercapacitor (Figure S2b). The HAC electrodes in a 1 M H_2SO_4 electrolyte retained the highest specific capacitance at a high current density of 10 A/g, demonstrating promising electrochemical properties suitable for supercapacitor electrodes, particularly in applications requiring a high energy density alongside a moderate power density. The HAC supercapacitor achieved a specific capacitance of 43.4 F/g at a current density of 10 A/g, resulting in an energy density of 6 Wh/kg (9.9 mWh/cm^3) and a power density of 5.5 kW/kg (9.1 W/cm^3).

Finally, the Ragone plot of the HAC supercapacitor is presented in Figure 9b. The HAC supercapacitor demonstrates excellent performance as a high-energy material capable of maintaining a relatively high energy density even at elevated power densities compared to AC derived from other biomass sources. Moreover, in comparison to advanced materials such as perovskites and MXene transition-metal sulfide composites,

https://doi.org/10.1021/acsomega.4c07518
ACS Omega 2025, 10, 6601−6614

the HAC supercapacitor achieves a higher power density while retaining a substantial energy density.

CONCLUSIONS

In conclusion, HAC has been successfully synthesized from hemp raw fiber by a chemical activation process using NaOH, with a mass ratio of biochar to NaOH is 1:4. The synthesized HAC was then characterized for its suitability as a supercapacitor electrode, with a comparison conducted among three different types of electrolytes: acidic (H_2SO_4), neutral (Na_2SO_4), and basic (KOH). Remarkably, the HAC electrode exhibited an exceptionally high specific capacitance of 594 F/g at a current density of 0.3 A/g in a 1 M H_2SO_4 electrolyte. The superior electrochemical performance of HAC, in comparison to commercial AC, can be attributed to its large surface area and the presence of oxygen functional groups on its surface. These features not only contribute to the electrical double-layer capacitance nature of AC but also provide pseudocapacitive behavior originating from the functional groups. Furthermore, HAC demonstrated the highest specific capacitance when immersed in the H_2SO_4 electrolyte. This can be attributed to the optimal size of its pores, as well as the optimal micro- and mesopore distribution in relation to the size of the hydrated ion. Notably, the maximum energy density and power density achieved by the HAC electrode were 82 Wh/kg (135.7 mWh/cm^3) and 188 W/kg (311 mW/cm^3), respectively, which are nearly twice as high as those of commercial AC. Additionally, the specific capacitance of the HAC symmetric supercapacitor, measured at a current density of 0.3 A/g, was approximately 138 F/g (228.3 F/cm^3), with the maximum energy density and power density of 19 Wh/kg (31.4 mWh/cm^3) and 165 W/kg (273 mW/cm^3), respectively. The excellent electrochemical performance of HAC indicates its potential as a cost-effective and high-performance electrode material, particularly when used with the H_2SO_4 electrolyte.

ASSOCIATED CONTENT

Supporting Information

The Supporting Information is available free of charge at https://pubs.acs.org/doi/10.1021/acsomega.4c07518.

Bode plot of the HAC electrode, measured in 1 M H_2SO_4, 3 M KOH, and 1 M Na_2SO_4 electrolytes, along with the specific capacitance plots at various current densities for the HAC electrode, AB520Y electrode, and HAC supercapacitor (PDF)

AUTHOR INFORMATION

Corresponding Author

Winadda Wongwiriyapan − *College of Materials Innovation and Technology, King Mongkut's Institute of Technology Ladkrabang, Bangkok 10520, Thailand;* orcid.org/0000-0002-0090-1664; Email: winadda.wo@kmitl.ac.th

Authors

Kanisorn Klangvijit − *College of Materials Innovation and Technology, King Mongkut's Institute of Technology Ladkrabang, Bangkok 10520, Thailand*

Khemjiranee Bowornthommatadsana − *College of Materials Innovation and Technology, King Mongkut's Institute of Technology Ladkrabang, Bangkok 10520, Thailand*

Mayuree Phonyiem Reilly − *College of Materials Innovation and Technology, King Mongkut's Institute of Technology Ladkrabang, Bangkok 10520, Thailand*

Teerayut Uwanno − *College of Materials Innovation and Technology, King Mongkut's Institute of Technology Ladkrabang, Bangkok 10520, Thailand*

Visittapong Yordsri − *National Metal and Materials Technology Center (MTEC), National Science and Technology Development Agency (NSTDA), Khlong Luang, Pathum Thani 12120, Thailand*

Michiko Obata − *Interdisciplinary Cluster for Cutting Edge Research, Research Initiative for Supra-Materials, Shinshu University, Nagano 380-8553, Japan*

Masatsugu Fujishige − *Global Aqua Innovation Center, Shinshu University, Nagano 380-8553, Japan; Faculty of Engineering, Shinshu University, Nagano 380-8553, Japan*

Kenji Takeuchi − *Interdisciplinary Cluster for Cutting Edge Research, Research Initiative for Supra-Materials, Shinshu University, Nagano 380-8553, Japan; Global Aqua Innovation Center, Shinshu University, Nagano 380-8553, Japan; Faculty of Engineering, Shinshu University, Nagano 380-8553, Japan;* orcid.org/0000-0002-5899-930X

Complete contact information is available at: https://pubs.acs.org/10.1021/acsomega.4c07518

Author Contributions

Conceptualization: M.P.R., T.U., and W.W.; Formal analysis: M.P.R., T.U., and W.W.; Funding acquisition: W.W.; Investigation: K.K., K.B., V.Y., and M.O.; Methodology: M.P.R., T.U., and W.W.; Project administration: K.T. and W.W.; Supervision: M.F. and K.T.; Validation: M.P.R., T.U., and W.W.; Writing—original draft: K.K.; Writing—review and editing: W.W. All authors have given approval to the final version of the manuscript.

Funding

The authors express their gratitude to the Office of National Higher Education Science Research and Innovation Policy Council (NXPO) (B05F640227) for providing financial support. Additionally, the research was partially funded through the King Mongkut's Institute of Technology Ladkrabang (KMITL) Doctoral Scholarship, granted to K.K.

Notes

The authors declare no competing financial interest.

ACKNOWLEDGMENTS

The authors are also thankful to the Nanotechnology and Material Analytical Instrument Service Unit (NMIS), College of Materials Innovation and Technology (CMIT), KMITL, for their valuable assistance. Furthermore, the authors acknowledge the support received from Eastern Spectrum Group Co., Ltd., in providing the hemp raw fiber for this study.

ABBREVIATIONS

HAC, hemp-activated carbon; EDLCs, electrochemical double-layer capacitors; LIBs, lithium-ion batteries; AC, activated carbon; PTFE, polytetrafluoroethylene; FESEM, field emission-scanning electron microscopy; BET, Brunauer−Emmett−Teller; DFT, density functional theory; XPS, X-ray photoelectron spectroscopy; TEM, transmission electron microscopy; XRD, X-ray diffraction; SAED, selected area electron diffraction pattern; CV, cyclic voltammetry; GCD, galvano-

https://doi.org/10.1021/acsomega.4c07518
ACS Omega 2025, 10, 6601−6614

static charge−discharge; EIS, electrochemical impedance spectroscopy

REFERENCES

(1) Burke, A. Ultracapacitors: why, how, and where is the technology. *J. Power Sources* **2000**, *91* (1), 37−50.

(2) Aricò, A. S.; Bruce, P.; Scrosati, B.; Tarascon, J.-M.; van Schalkwijk, W. Nanostructured materials for advanced energy conversion and storage devices. *Nat. Mater.* **2005**, *4* (5), 366−377.

(3) Chu, A.; Braatz, P. Comparison of commercial supercapacitors and high-power lithium-ion batteries for power-assist applications in hybrid electric vehicles: I. Initial characterization. *J. Power Sources* **2002**, *112* (1), 236−246.

(4) Zhang, L. L.; Zhao, X. S. Carbon-based materials as supercapacitor electrodes. *Chem. Soc. Rev.* **2009**, *38* (9), 2520−2531 10.1039/B813846J..

(5) Ukkakimapan, P.; Sattayarut, V.; Wanchaem, T.; Yordsri, V.; Phonyiem, M.; Ichikawa, S.; Obata, M.; Fujishige, M.; Takeuchi, K.; Wongwiriyapan, W.; Endo, M. Preparation of activated carbon via acidic dehydration of durian husk for supercapacitor applications. *Diamond Relat. Mater.* **2020**, *107*, No. 107906.

(6) Ukkakimapan, P.; Ukakimaparn, P.; Wanchaem, T.; Yordsri, V.; Sattayarut, V.; Phonyiem, M.; Fujishige, M.; Takeuchi, K.; Wongwiriyapan, W. Investigation on electrochemical properties of sugarcane leaves-derived activated carbon by steam activation. *Solid State Phenom.* **2020**, *302*, 63−70, DOI: 10.4028/www.scientific.net/SSP.302.63.

(7) Yu, G.; Hu, L.; Vosgueritchian, M.; Wang, H.; Xie, X.; McDonough, J. R.; Cui, X.; Cui, Y.; Bao, Z. Solution-Processed Graphene/MnO2 Nanostructured Textiles for High-Performance Electrochemical Capacitors. *Nano Lett.* **2011**, *11* (7), 2905−2911.

(8) Jeong, J.-H.; Park, J. W.; Lee, D. W.; Baughman, R. H.; Kim, S. J. Electrodeposition of α-MnO2/γ-MnO2 on Carbon Nanotube for Yarn Supercapacitor. *Sci. Rep.* **2019**, *9* (1), No. 11271.

(9) Jiang, M.; Liu, Z.; Hu, J.; Liu, Y.; Luo, Y.; Lai, X.; Xu, T. Facile electrodeposition of Mn3O4 nanoparticles on wood-derived porous carbon for high-performance asymmetric supercapacitor. *Diamond Relat. Mater.* **2021**, *118*, No. 108506.

(10) Liu, G. F.; Ma, P. P.; Qiao, Y.; Xu, R. H.; Huang, D. M.; Hu, R. Y.; Liu, L. Y.; Jiang, G. H.; Demir, M. Perovskite SrCo1-xTixO3-δ as anion-intercalated electrode materials for supercapacitors. *J. Energy Storage* **2022**, *52*, No. 104942.

(11) Liu, G.; Liu, L.; Li, G.; Wu, S.; He, J.; Zhou, Y.; Demir, M.; Ma, P. Temperature-Dependent Electrochemical Performance of Ta-Substituted SrCoO3 Perovskite for Supercapacitors. *Chem. - Eur. J.* **2024**, *30* (14), No. e202303267.

(12) Zhang, Y.; Ding, J.; Xu, W.; Wang, M.; Shao, R.; Sun, Y.; Lin, B. Mesoporous LaFeO3 perovskite derived from MOF gel for all-solid-state symmetric supercapacitors. *Chem. Eng. J.* **2020**, *386*, No. 124030.

(13) Laforgue, A.; Simon, P.; Fauvarque, J. F.; Mastragostino, M.; Soavi, F.; Sarrau, J. F.; Lailler, P.; Conte, M.; Rossi, E.; Saguatti, S. Activated Carbon/Conducting Polymer Hybrid Supercapacitors. *J. Electrochem. Soc.* **2003**, *150* (5), A645.

(14) Vighnesha, K.; Shruthi; Sandhya; Sangeetha, D.; Selvakumar, M. Synthesis and characterization of activated carbon/conducting polymer composite electrode for supercapacitor applications. *J. Mater. Sci.: Mater. Electron.* **2018**, *29*, 914−921.

(15) Potphode, D. D.; Mishra, S. P.; Sivaraman, P.; Patri, M. Asymmetric supercapacitor devices based on dendritic conducting polymer and activated carbon. *Electrochim. Acta* **2017**, *230*, 29−38.

(16) Teo, E. Y. L.; Muniandy, L.; Ng, E.-P.; Adam, F.; Mohamed, A. R.; Jose, R.; Chong, K. F. High surface area activated carbon from rice husk as a high performance supercapacitor electrode. *Electrochim. Acta* **2016**, *192*, 110−119.

(17) Su, X.-L.; Cheng, M.-Y.; Fu, L.; Yang, J.-H.; Zheng, X.-C.; Guan, X.-X. Superior supercapacitive performance of hollow activated carbon nanomesh with hierarchical structure derived from poplar catkins. *J. Power Sources* **2017**, *362*, 27−38.

(18) Roy, C. K.; Shah, S. S.; Reaz, A. H.; Sultana, S.; Chowdhury, A. N.; Firoz, S. H.; Zahir, M. H.; Ahmed Qasem, M. A.; Aziz, M. A. Preparation of hierarchical porous activated carbon from banana leaves for high-performance supercapacitor: effect of type of electrolytes on performance. *Chem. - Asian J.* **2021**, *16* (4), 296−308.

(19) Pandolfo, A. G.; Hollenkamp, A. F. Carbon properties and their role in supercapacitors. *J. Power Sources* **2006**, *157* (1), 11−27.

(20) Wang, Y.; Shi, Z.; Huang, Y.; Ma, Y.; Wang, C.; Chen, M.; Chen, Y. Supercapacitor Devices Based on Graphene Materials. *J. Phys. Chem. C* **2009**, *113* (30), 13103−13107.

(21) Zhang, T.; Fuchs, B.; Secchiaroli, M.; Wohlfahrt-Mehrens, M.; Dsoke, S. Electrochemical behavior and stability of a commercial activated carbon in various organic electrolyte combinations containing Li-salts. *Electrochim. Acta* **2016**, *218*, 163−173.

(22) Sattayarut, V.; Chanthad, C.; Khemthong, P.; Kuboon, S.; Wanchaem, T.; Phonyiem, M.; Obata, M.; Fujishige, M.; Takeuchi, K.; Wongwiriyapan, W.; et al. Preparation and electrochemical performance of nitrogen-enriched activated carbon derived from silkworm pupae waste. *RSC Adv.* **2019**, *9* (18), 9878−9886.

(23) Sattayarut, V.; Wanchaem, T.; Ukkakimapan, P.; Yordsri, V.; Dulyaseree, P.; Phonyiem, M.; Obata, M.; Fujishige, M.; Takeuchi, K.; Wongwiriyapan, W.; Endo, M. Nitrogen self-doped activated carbons via the direct activation of *Samanea saman* leaves for high energy density supercapacitors. *RSC Adv.* **2019**, *9* (38), 21724−21732.

(24) Fuertes, A.; Lota, G.; Centeno, T.; Frackowiak, E. Templated mesoporous carbons for supercapacitor application. *Electrochim. Acta* **2005**, *50* (14), 2799−2805.

(25) Ismar, E.; Karazehir, T.; Ates, M.; Sarac, A. S. Electrospun carbon nanofiber web electrode: Supercapacitor behavior in various electrolytes. *J. Appl. Polym. Sci.* **2018**, *135* (4), No. 45723.

(26) Lu, W.; Dai, L. Carbon Nanotube Supercapacitors. In *Carbon Nanotubes*; IntechOpen, 2010.

(27) Muangrat, W.; Obata, M.; Htay, M. T.; Fujishige, M.; Dulyaseree, P.; Wongwiriyapan, W.; Hashimoto, Y. Nitrogen-doped graphene nanosheet-double-walled carbon nanotube hybrid nanostructures for high-performance supercapacitors. *FlatChem* **2021**, *29*, No. 100292.

(28) Wang, X.; Liu, L.; Wang, X.; Bai, L.; Wu, H.; Zhang, X.; Yi, L.; Chen, Q. Preparation and performances of carbon aerogel microspheres for the application of supercapacitor. *J. Solid State Electrochem.* **2011**, *15*, 643−648.

(29) Velasco, A.; Ryu, Y. K.; Boscá, A.; Ladrón-de-Guevara, A.; Hunt, E.; Zuo, J.; Pedrós, J.; Calle, F.; Martinez, J. Recent trends in graphene supercapacitors: from large area to microsupercapacitors. *Sustainable Energy Fuels* **2021**, *5* (5), 1235−1254.

(30) Zhang, G.; Chen, Y.; Chen, Y.; Guo, H. Activated biomass carbon made from bamboo as electrode material for supercapacitors. *Mater. Res. Bull.* **2018**, *102*, 391−398.

(31) Fujishige, M.; Yoshida, I.; Toya, Y.; Banba, Y.; Oshida, K.-i.; Tanaka, Y.-s.; Dulyaseree, P.; Wongwiriyapan, W.; Takeuchi, K. Preparation of activated carbon from bamboo-cellulose fiber and its use for EDLC electrode material. *J. Environ. Chem. Eng.* **2017**, *5* (2), 1801−1808.

(32) Dulyaseree, P.; Fujishige, M.; Yoshida, I.; Toya, Y.; Banba, Y.; Tanaka, Y.-s.; Aoyama, T.; Phonyiem, M.; Wongwiriyapan, W.; Takeuchi, K.; Endo, M. Nitrogen-rich green leaves of papaya and Coccinia grandis as precursors of activated carbon and their electrochemical properties. *RSC Adv.* **2017**, *7* (67), 42064−42072.

(33) Niu, L.; Shen, C.; Yan, L.; Zhang, J.; Lin, Y.; Gong, Y.; Li, C.; Sun, C. Q.; Xu, S. Waste bones derived nitrogen−doped carbon with high micropore ratio towards supercapacitor applications. *J. Colloid Interface Sci.* **2019**, *547*, 92−101.

(34) Mu, J.; Wong, S. I.; Li, Q.; Zhou, P.; Zhou, J.; Zhao, Y.; Sunarso, J.; Zhuo, S. Fishbone-derived N-doped hierarchical porous carbon as an electrode material for supercapacitor. *J. Alloys Compd.* **2020**, *832*, No. 154950.

(35) Zeng, L.; Lou, X.; Zhang, J.; Wu, C.; Liu, J.; Jia, C. Carbonaceous mudstone and lignin-derived activated carbon and its

https://doi.org/10.1021/acsomega.4c07518
ACS Omega 2025, 10, 6601−6614

application for supercapacitor electrode. *Surf. Coat. Technol.* **2019**, *357*, 580−586.
(36) Zhao, Z.; Hao, S.; Hao, P.; Sang, Y.; Manivannan, A.; Wu, N.; Liu, H. Lignosulphonate-cellulose derived porous activated carbon for supercapacitor electrode. *J. Mater. Chem. A* **2015**, *3* (29), 15049−15056.
(37) Sharma, P.; Singh, D.; Minakshi, M.; Quadsia, S.; Ahuja, R. Activation-Induced Surface Modulation of Biowaste-Derived Hierarchical Porous Carbon for Supercapacitors. *ChemPlusChem* **2022**, *87* (6), No. e202200126.
(38) Wickramaarachchi, K.; Minakshi, M.; Aravindh, S. A.; Dabare, R.; Gao, X.; Jiang, Z.-T.; Wong, K. W. Repurposing N-Doped Grape Marc for the Fabrication of Supercapacitors with Theoretical and Machine Learning Models. *Nanomaterials* **2022**, *12* (11), No. 1847, DOI: 10.3390/nano12111847.
(39) Wickramaarachchi, W. A. M. K. P.; Minakshi, M.; Gao, X.; Dabare, R.; Wong, K. W. Hierarchical porous carbon from mango seed husk for electro-chemical energy storage. *Chem. Eng. J. Adv.* **2021**, *8*, No. 100158.
(40) Gao, Y.; Yue, Q.; Gao, B.; Li, A. Insight into activated carbon from different kinds of chemical activating agents: A review. *Sci. Total Environ.* **2020**, *746*, No. 141094.
(41) Jiang, X.; Shi, G.; Wang, G.; Mishra, P.; Liu, C.; Dong, Y.; Zhang, P.; Tian, H.; Liu, Y.; Wang, Z.; et al. A hydrothermal carbonization process for the preparation of activated carbons from hemp straw: an efficient electrode material for supercapacitor application. *Ionics* **2019**, *25* (7), 3299−3307.
(42) Rosas, J. M.; Bedia, J.; Rodríguez-Mirasol, J.; Cordero, T. Preparation of Hemp-Derived Activated Carbon Monoliths. Adsorption of Water Vapor. *Ind. Eng. Chem. Res.* **2008**, *47* (4), 1288−1296.
(43) Sun, W.; Lipka, S. M.; Swartz, C.; Williams, D.; Yang, F. Hemp-derived activated carbons for supercapacitors. *Carbon* **2016**, *103*, 181−192 Scopus..
(44) Zhang, J.; Duan, Y.; Jiang, Z.; Chen, T.; Wang, K.; Wang, K.; Zhang, W.; Hu, J. Investigation of the supercapacitance of ruthenium-based/hemp stem activated carbon. *J. Phys. Chem. Solids* **2021**, *153*, No. 110019.
(45) Amran, F.; Zaini, M. A. A. Effects of chemical activating agents on physical properties of activated carbons−a commentary. *Water Pract. Technol.* **2020**, *15* (4), 863−876.
(46) Tongpoothorn, W.; Sriuttha, M.; Homchan, P.; Chanthai, S.; Ruangviriyachai, C. Preparation of activated carbon derived from Jatropha curcas fruit shell by simple thermo-chemical activation and characterization of their physico-chemical properties. *Chem. Eng. Res. Des.* **2011**, *89* (3), 335−340.
(47) Yang, R.; Liu, G.; Xu, X.; Li, M.; Zhang, J.; Hao, X. Surface texture, chemistry and adsorption properties of acid blue 9 of hemp (*Cannabis sativa* L.) bast-based activated carbon fibers prepared by phosphoric acid activation. *Biomass Bioenergy* **2011**, *35* (1), 437−445.
(48) Hossain, M. Z.; Wu, W.; Xu, W. Z.; Chowdhury, M. B. I.; Jhawar, A. K.; Machin, D.; Charpentier, P. A. High-Surface-Area Mesoporous Activated Carbon from Hemp Bast Fiber Using Hydrothermal Processing. *C* **2018**, *4* (3), 38.
(49) Zhong, C.; Deng, Y.; Hu, W.; Qiao, J.; Zhang, L.; Zhang, J. A review of electrolyte materials and compositions for electrochemical supercapacitors. *Chem. Soc. Rev.* **2015**, *44* (21), 7484−7539.
(50) Pal, B.; Yang, S.; Ramesh, S.; Thangadurai, V.; Jose, R. Electrolyte selection for supercapacitive devices: a critical review. *Nanoscale Adv.* **2019**, *1* (10), 3807−3835.
(51) Béguin, F.; Presser, V.; Balducci, A.; Frackowiak, E. Carbons and Electrolytes for Advanced Supercapacitors. *Adv. Mater.* **2014**, *26* (14), 2219−2251.
(52) Thommes, M.; Kaneko, K.; Neimark, A. V.; Olivier, J. P.; Rodriguez-Reinoso, F.; Rouquerol, J.; Sing, K. S. W. Physisorption of gases, with special reference to the evaluation of surface area and pore size distribution (IUPAC Technical Report). *Pure Appl. Chem.* **2015**, *87* (9−10), 1051−1069, DOI: 10.1515/pac-2014-1117.
(53) Su, X.-L.; Li, S.-H.; Jiang, S.; Peng, Z.-K.; Guan, X.-X.; Zheng, X.-C. Superior capacitive behavior of porous activated carbon tubes derived from biomass waste-cotonier strobili fibers. *Adv. Powder Technol.* **2018**, *29* (9), 2097−2107.
(54) Liu, X.-Y.; Huang, M.; Ma, H.-L.; Zhang, Z.-Q.; Gao, J.-M.; Zhu, Y.-L.; Han, X.-J.; Guo, X.-Y. Preparation of a Carbon-Based Solid Acid Catalyst by Sulfonating Activated Carbon in a Chemical Reduction Process. *Molecules* **2010**, *15* (10), 7188−7196.
(55) Wei, Z.; Pan, R.; Hou, Y.; Yang, Y.; Liu, Y. Graphene-supported Pd catalyst for highly selective hydrogenation of resorcinol to 1, 3-cyclohexanedione through giant π-conjugate interactions. *Sci. Rep.* **2015**, *5* (1), No. 15664.
(56) Seah, M. P. The quantitative analysis of surfaces by XPS: A review. *Surf. Interface Anal.* **1980**, *2* (6), 222−239.
(57) Yang, D.; Velamakanni, A.; Bozoklu, G.; Park, S.; Stoller, M.; Piner, R. D.; Stankovich, S.; Jung, I.; Field, D. A.; Ventrice, C. A.; Ruoff, R. S. Chemical analysis of graphene oxide films after heat and chemical treatments by X-ray photoelectron and Micro-Raman spectroscopy. *Carbon* **2009**, *47* (1), 145−152.
(58) Wickramaarachchi, K.; Sundaram, M. M.; Henry, D. Surfactant-mediated electrodeposition of a pseudocapacitive manganese dioxide a twofer. *J. Energy Storage* **2022**, *55*, No. 105403.
(59) Minakshi, M.; Wickramaarachchi, K. Electrochemical aspects of supercapacitors in perspective: From electrochemical configurations to electrode materials processing. *Prog. Solid State Chem.* **2023**, *69*, No. 100390.
(60) Mendhe, A.; Panda, H. S. A review on electrolytes for supercapacitor device. *Discover Mater.* **2023**, *3* (1), 29.
(61) Wu, Z.-S.; Winter, A.; Chen, L.; Sun, Y.; Turchanin, A.; Feng, X.; Müllen, K. Three-Dimensional Nitrogen and Boron Co-doped Graphene for High-Performance All-Solid-State Supercapacitors. *Adv. Mater.* **2012**, *24* (37), 5130−5135.
(62) Yoon, B.-J.; Jeong, S.-H.; Lee, K.-H.; Kim, H. S.; Park, C. G.; Han, J. H. Electrical properties of electrical double layer capacitors with integrated carbon nanotube electrodes. *Chem. Phys. Lett.* **2004**, *388* (1), 170−174.
(63) Wang, S.; Zhang, J.; Shang, P.; Li, Y.; Chen, Z.; Xu, Q. N-doped carbon spheres with hierarchical micropore-nanosheet networks for high performance supercapacitors. *Chem. Commun.* **2014**, *50* (81), 12091−12094 10.1039/C4CC04832F..
(64) Kim, Y. J.; Abe, Y.; Yanagiura, T.; Park, K. C.; Shimizu, M.; Iwazaki, T.; Nakagawa, S.; Endo, M.; Dresselhaus, M. S. Easy preparation of nitrogen-enriched carbon materials from peptides of silk fibroins and their use to produce a high volumetric energy density in supercapacitors. *Carbon* **2007**, *45* (10), 2116−2125.
(65) Senthilkumar, S. T.; Senthilkumar, B.; Balaji, S.; Sanjeeviraja, C.; Selvan, R. K. Corrigendum to "Preparation of activated carbon from sorghum pith and its structural and electrochemical properties" [Mater. Res. Bull. 46 (2011) 413−419]. *Mater. Res. Bull.* **2011**, *46* (8), 1320.
(66) Zhang, J.; Zhang, X.; Zhou, Y.; Guo, S.; Wang, K.; Liang, Z.; Xu, Q. Nitrogen-Doped Hierarchical Porous Carbon Nanowhisker Ensembles on Carbon Nanofiber for High-Performance Supercapacitors. *ACS Sustainable Chem. Eng.* **2014**, *2* (6), 1525−1533.
(67) Rufford, T. E.; Hulicova-Jurcakova, D.; Zhu, Z.; Lu, G. Q. Nanoporous carbon electrode from waste coffee beans for high performance supercapacitors. *Electrochem. Commun.* **2008**, *10* (10), 1594−1597.
(68) Kötz, R.; Carlen, M. Principles and applications of electrochemical capacitors. *Electrochim. Acta* **2000**, *45* (15), 2483−2498.
(69) Nightingale, E. R., Jr. Phenomenological Theory of Ion Solvation. Effective Radii of Hydrated Ions. *J. Phys. Chem. A* **1959**, *63* (9), 1381−1387.
(70) Volkov, A. G.; Paula, S.; Deamer, D. W. Two mechanisms of permeation of small neutral molecules and hydrated ions across phospholipid bilayers. *Bioelectrochem. Bioenerg.* **1997**, *42* (2), 153−160.
(71) Huang, J.; Sumpter, B. G.; Meunier, V. A Universal Model for Nanoporous Carbon Supercapacitors Applicable to Diverse Pore Regimes, Carbon Materials, and Electrolytes. *Chem. - Eur. J.* **2008**, *14* (22), 6614−6626.

https://doi.org/10.1021/acsomega.4c07518
ACS Omega 2025, 10, 6601−6614

(72) Guo, S.; Liang, Y.; Zhou, Q. Complement and correction for meta-analysis of patients with extensive-stage small cell lung cancer managed with irinotecan/cisplatin versus etoposide/cisplatin as first-line chemotherapy. *J. Thorac. Oncol.* **2011**, *6* (2), 406−408.
(73) Barzegar, F.; Momodu, D. Y.; Fashedemi, O. O.; Bello, A.; Dangbegnon, J. K.; Manyala, N. Investigation of different aqueous electrolytes on the electrochemical performance of activated carbon-based supercapacitors. *RSC Adv.* **2015**, *5* (130), 107482−107487 10.1039/C5RA21962K..
(74) Rajasekaran, S. J.; Grace, A. N.; Jacob, G.; Alodhayb, A.; Pandiaraj, S.; Raghavan, V. Investigation of Different Aqueous Electrolytes for Biomass-Derived Activated Carbon-Based Supercapacitors. *Catalysts* **2023**, *13* (2), 286.
(75) Largeot, C.; Portet, C.; Chmiola, J.; Taberna, P.-L.; Gogotsi, Y.; Simon, P. Relation between the Ion Size and Pore Size for an Electric Double-Layer Capacitor. *J. Am. Chem. Soc.* **2008**, *130* (9), 2730−2731.
(76) Wang, J.; Polleux, J.; Lim, J.; Dunn, B. Pseudocapacitive Contributions to Electrochemical Energy Storage in TiO2 (Anatase) Nanoparticles. *J. Phys. Chem. C* **2007**, *111* (40), 14925−14931.
(77) Shao, Y.; El-Kady, M. F.; Sun, J.; Li, Y.; Zhang, Q.; Zhu, M.; Wang, H.; Dunn, B.; Kaner, R. B. Design and Mechanisms of Asymmetric Supercapacitors. *Chem. Rev.* **2018**, *118* (18), 9233−9280.
(78) Gunasekaran, S. S.; Badhulika, S. High-performance solid-state supercapacitor based on sustainable synthesis of meso-macro porous carbon derived from hemp fibres via CO2 activation. *J. Energy Storage* **2021**, *41*, No. 102997.
(79) Jiang, X.; Shi, G.; Wang, G.; Mishra, P.; Du, J.; Zhang, Y. Fe2O3/hemp straw-based porous carbon composite for supercapacitor electrode materials. *Ionics* **2020**, *26* (8), 4039−4051.

https://doi.org/10.1021/acsomega.4c07518
ACS Omega 2025, 10, 6601−6614